Soft Matter

REVIEW

Soft diffuse interfaces in electrokinetics – theory and experiment for transport in charged diffuse layers

Alexander C. Barbati and Brian J. Kirby*

Charged and uncharged soft interfaces are present in a variety of microfluidic and biological systems. The electrokinetic properties of these fixed-diffuse-charge systems are dependent on (1) the components of the working fluid, (2) the bounding surface of the diffuse charge layer, and (3) the chemical and mechanical properties of the film itself. Here, we describe recent and past literature to provide a framework for the interpretation of data, utilizing the electrokinetic coupling matrix, and a description of the experimental techniques relevant for microfluidic systems. In this work, we focus on experiments on, and models for, flat surfaces with constant film mass.

1 Introduction

Soft materials occur throughout natural and synthetic systems. In biology, soft materials are present inside and outside most multicellular organisms, found at the boundaries of the tissue and vasculature.[1] Less complex organisms, such as bacteria, have diffuse charge layers on their outer surface that are essential for cell adhesion[2–4] and other processes.[5] In the lab, both charged and uncharged polymer layers may be grafted to structures and within capillaries to suppress electroosmosis,[6,7] or otherwise modify the surface chemistry and charge.[7,8] Despite the ubiquity of these interfaces, our ability to describe fixed-diffuse-charge systems is limited by ambiguities in the electrostatic and hydrodynamic governing equations and associated boundary conditions.

Descriptions of electrokinetic (EK) phenomena generally depend upon the ζ-potential of the material–solution system. The ζ-potential relates to the surface potential, ϕ_o, which is a critical component of DLVO theory used to characterize the interaction between charged surfaces;[9,10] ζ is furthermore used to predict

Sibley School of Mechanical and Aerospace Engineering, Cornell University, Ithaca, NY 14853, USA. Tel: +1-607-255-1222. Fax: +1-607-255-4379. E-mail: kirby@cornell.edu

electroosmotic fluid actuation in glass and polymer capillaries.[11,12] Electrokinetic characterization of the ζ-potential for a range of solution conditions is relatively straightforward for rigid-walled systems because the electrostatic and hydrodynamic boundaries coincide; for soft interfaces this is often not the case. Here and throughout we consider a soft interface to be a system composed of a rigid backing wall upon which a fluid permeable layer resides. These layers may be charged or uncharged.

A complete description of soft interfaces requires that we consider four key points:

(1) *Chemical interactions between the diffuse-charge layer and the bulk fluid.* We must know film chemistry to predict film charge as a function of pH and ionic strength. Oxides can have poorly defined dissociation chemistries and charging behavior[11] but polymer and other films can be synthesized or selected to create systems with improved chemical definition, using tuned acid/base dissociation constants. Furthermore, models can be formulated and validated against experiments to extract key chemical parameters (*e.g.*, active site density, pK_a of surface groups). Questions remain, however, with the charge-generating mechanism of chemically inert polymers and underlying rigid film backing.

Alexander Barbati is a graduate student at Cornell University in the Micro/Nanofluidics laboratory; he received a B.S. in mechanical engineering from the University of Massachusetts at Amherst in 2007. He has worked on the design and construction of devices for neural culture, as well as fundamentals and modeling of electrokinetic transport for microfluidic devices. More generally, his research interest include small-scale transport phenomena, electrokinetics, and electrochemistry in microfluidic systems.

Brian Kirby's research interests include transport in microfluidic devices with a disciplinary focus on electrokinetics and application interests primarily in cellular bioanalysis. He was educated at the University of Michigan and Stanford, worked in a microfluidic counterbioterrorism group at Sandia National Laboratories, and has taught in the Sibley School of Mechanical and Aerospace Engineering at Cornell since 2004. He has authored a leading textbook on microscale fluid mechanics, and has taught the physics of micro- and nanoscale fluid mechanics at Cornell since 2005.

(2) *Mechanical interaction models between the diffuse-fixed-charge layer and the bulk fluid.* Fluid–film interactions govern pressure- and electroosmotically-driven transport. Models of fluid–solid interaction for films as a function of pH, ionic strength, temperature and other local solvent/film properties must be composed to describe the transport of fluid within the film layer. The solution to this problem will enable descriptions of momentum transfer in films, likely using an effective viscosity or Brinkman-type correction to the Navier–Stokes equations.

(3) *Modeling of the surface- and fluid-generated potential field.* Closed-form solution for film potentials are known only in specific limits of relative film size (relative to the Debye length) and film potential (relative to the thermal voltage). Films may be described with variable or uniform charge, and coupled to the governing Poisson–Boltzmann equation as a forcing term as a function of space. Potential modeling of the film and fluid are necessary to quantify charge and momentum transport. As in solid-surface electrokinetics, analyses can be simplified in the low-potential linear case, or examined numerically in the nonlinear case.

(4) *Experimental methods to extract film–fluid system parameters.* Experiments are required to validate proposed theories. Relevant experimental measurables for films on solid substrates in microfluidic systems are electroosmotic velocity induced by an electric field transverse to the film surface normal, conductance of the film, and measured streaming current and potential. Contemporary advances in microfabrication techniques, metrology tools such as AFM,[13] and the wealth of physical and chemical information on polymer films encourages parametric investigations of solid–film–solution systems to test quantitatively proposed models for these systems.

Here, we address these aspects of the solid–film–fluid interface for applications in microfluidic systems; specific attention is paid to the coupling of film properties using the formalism of the electrokinetic coupling matrix. Recently, Pallandre, *et al.*[14] reviewed aspects of these systems, with regard to the application of surface treatment techniques developed for large surfaces. Zembala reviewed electrokinetics of heterogeneous surfaces,[15] examining diffuse charge layers on heterogeneous particles and electrokinetics of particles adsorbed on surfaces. A later review by Adamczyk and co-workers[16] describes work on heterogeneous surfaces, considering more specifically the case of particle covered surfaces with well-defined ζ-potentials.

In the first half of this paper, we review fundamental electrokinetics of rigid surfaces, and then incorporate the ideas of diffuse interfaces to compare between the two. In the second half, we review the literature in two parts: (i) theoretical descriptions of diffuse interfaces and (ii) experimental work on diffuse interfaces. We conclude with future directions in diffuse interface research.

2 Theoretical electrokinetics at hard and soft interfaces

2.1 Fundamentals of electrokinetics at hard and soft interfaces

The ζ-potential is of fundamental interest and importance in electrokinetics, representing the observed electrokinetic potential as the result of an experiment. The ζ-potential stands in contrast to the surface potential, ϕ_o (Fig. 1), which is the electrical potential of the coincident plane at the solid surface. Commonly, as in the case
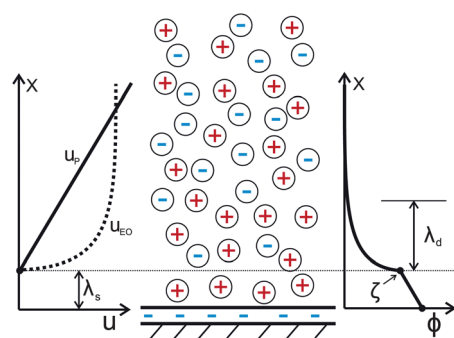

Fig. 1 Diagram of charge-generated potential profiles at an impermeable charged interface. Bound wall charge (here negative) generates an immobile (Stern) layer of ions and a diffuse layer. Schematic potential and velocity profiles, as a result of forcing by pressure and potential fields, illustrate characteristic length scales and behaviors. The velocity profiles at left are comparable in shape but not magnitude.

of the Gouy–Chapman model,[17] the two are taken to coincide. In the Gouy–Chapman–Stern model the two potentials are different; an immobile layer of ions with thickness λ_s offsets the plane of shear and surface potential, as shown in Fig. 1.

The starting point for the analysis of double-layer phenomena is the Poisson–Boltzmann equation:

$$\nabla \cdot (-\varepsilon^* \varepsilon_o \nabla \phi) = \rho_e + \rho_f = F \sum_{j=1}^n c_{j,\infty} z_j^* e^{\frac{-z_j^* F\phi}{RT}} + \rho_f \qquad (1)$$

here, ϕ is the electrical potential, ε_o is the permittivity of free space, ε^* is the dielectric constant in the continuum, F is Faraday's constant, $c_{j,\infty}$ and z_j^* are the bulk concentration and valence for the jth ionic component (from a total of n), R is the molar gas constant, T the temperature, ρ_e is the free charge density (expressed *via* the Boltzmann distribution in eqn (1)), and ρ_f is the fixed charge density. Unitless variables are embellished with asterisks; dimensionless functions and non-dimensional parameters (*e.g.*, Du) are, however, *not* embellished. The Poisson–Boltzmann equation is nondimensionalized by the Debye length $\lambda_d = \sqrt{\frac{\varepsilon^* \varepsilon_o RT}{2F^2 I_c}}$, the characteristic electrical decay length in the fluid, the thermal voltage $\phi_T = \frac{RT}{F} \sim 25$ [mV] as the characteristic potential, the ionic strength $I_c = 1/2 \sum_{j=1}^n z_j^{*2} c_{j,\infty}$ as a concentration scale, and an arbitrary parameter, β, as a scale for the fixed charge. For a $z^*:z^*$ electrolyte with uniform permittivity, the 1-D Poisson–Boltzmann equation becomes:

$$\frac{d^2\phi^*}{dx^{*2}} = -\frac{1}{z^*}\sinh(z^*\phi^*) - \rho_f^*(x)\frac{\beta}{2FI_c} \qquad (2)$$

Eqn (2) above suggests the scale β be taken as $2FI_c$, which is characteristic of the charge capacity of the ions in solution. Dukhin, *et al.*[18] has additionally proposed a length scale for characteristic electrical decay *within* the fixed charge layer:

$$\lambda_\delta = \lambda_d \sqrt{\frac{2Fc_\infty}{|\rho_f|}} = \sqrt{\frac{\varepsilon^* \varepsilon_o RT}{F|\rho_f|}} \qquad (3)$$

This relation communicates the importance of the fixed charge on the electrical potential profiles, and is paramount in

descriptions of conductivity within the film. In the absence of a charged layer, $\rho_f(x) = 0$, the boundary condition on the solid wall is described with either a fixed charge, $\varepsilon^* \varepsilon_o \left. \frac{d\phi}{dx} \right|_{x=0}$, or a fixed potential, ϕ_o. The second boundary condition in bulk solution or the far field is taken to have zero charge or zero field, or, in the case of symmetrical walls, a second fixed charge or fixed potential.

The ζ-potential is the electrokinetic potential at or near the rigid surface, and it is obtained from an electrokinetic experiment, *e.g.*, streaming current/potential,[11,19,20] current monitoring,[11,19,20] or neutral-dye elution.[11,19,20] A variety of other techniques may be used, including surface conductance or dielectric spectroscopy measurements.[21] Streaming current/potential and conductance techniques are the most useful for these studies, as the chemistry of the working fluid remains constant and the required equipment is readily available.

Streaming current and streaming potential techniques are straightforward to interpret on rigid surfaces in the thin-EDL limit. In a streaming-type experiment, the test cell is typically a small-bore (diameter typically 25 to 150 μm) capillary[22–25] or parallel plate assembly.[26–28] Fluid is actuated by a pressure difference, Δp, across the channel of length ℓ and uniform area A. The pressure difference generates a flow with velocity field $\boldsymbol{u}$ that acts to transport the free charge density (ρ_e) as a current:

$$I_{str} = \int_A \boldsymbol{u} \rho_e \cdot dA$$

When the hydraulic radius of the channel, $r_h \sim 2 \times$ area/perimeter is large relative to the Debye length, the streaming current integrates to:[19,29]

$$I_{str} = \frac{\zeta \varepsilon^* \varepsilon_o A}{\eta} \frac{\Delta p}{\ell} \qquad (5)$$

Thus, the channel cross-section and fluid properties are known, and we can measure the streaming current and pressure drop across the channel to yield an expression for the ζ-potential. A similar technique, streaming potential, uses the same experimental setup, but the electrical potential is measured with a high-impedance voltmeter rather than current with a low-impedance ammeter. In enforcing $I = 0$, an adverse current of charged species is conducted through the fluid as caused by an equilibrium E-field.

The mechanism of system conductance is essential to the measured streaming potential. Absent double layer effects, the system conductance is due only to the presence of ions in the bulk fluid, although surface conductance effects can be present owing to the charged surface. The presence of the surface enhances the conductivity of the system. The total effective conductivity of the channel is a combination of the bulk and surface conductivities:

$$\sigma = \sigma_B + \frac{G_s}{r_h} \qquad (6)$$

where σ is the system conductivity, σ_B the conductivity of the bulk fluid, and G_s the surface conductance. By recasting the total conductivity, we extract a nondimensional parameter that defines the relative importance of the surface conductance:

$$\sigma = \sigma_B(1 + Du) \qquad (7)$$

The Dukhin number is defined as $Du = G_s/\sigma_B r_h$. As the characteristic dimension of the channel and solution ionic strength increases, surface conductance effects become less apparent – Davies and Rideal remark,[30] that capillary ζ-potentials were initially thought to depend on the radius of the capillary directly only to be later understood as enhanced conductivity as the surface to volume ratio of the capillary increased. Attempts at analytical descriptions of the surface conductance tend to underestimate the observed values.[31–34]

The surface conductance of a system may be determined in several ways. Common methods are (a) the four-electrode technique of Schwan and Ferris,[35] which is a direct measurement of the cell conductivity, (b) a limiting extrapolation method in which an electrokinetic measurement is performed as the characteristic channel dimension is changed, and (c) sequential streaming current and streaming potential measurements from which the cell conductivity is derived and corrected by the bulk fluid value.

2.2 The electrokinetic coupling matrix

The cognate electrokinetic phenomena are well described with formalism of the electrokinetic coupling matrix.[19,36] Here, the system is forced by a pressure gradient $\nabla p \cdot \vec{n}$, with $\vec{n}$ directed along the channel axis, and/or an electric field E, and the outputs are flow and/or current densities. Generally,

$$\begin{bmatrix} Q/A \\ I/A \end{bmatrix} = \begin{bmatrix} \chi_{11} & \chi_{12} \\ \chi_{21} & \chi_{22} \end{bmatrix} \begin{bmatrix} -\nabla p \cdot \vec{n} \\ E \end{bmatrix} \qquad (8)$$

This matrix communicates immediately all essential electrokinetic phenomena: fluid flow in the absence of electrical forcing depends on χ_{11} only ($Q/A = -\chi_{11}\nabla p \cdot \vec{n}$), streaming current depends on χ_{21} only ($I/A = -\chi_{21}\nabla p \cdot \vec{n}$), conductivity measurements on χ_{22} only ($I/A = \chi_{22}E$), and streaming potential on a ratio of χ_{22} and χ_{21} ($I/A = 0 \Rightarrow E = \chi_{21}/\chi_{22}\nabla p \cdot \vec{n}$). Other phenomena such as EK pumping ($-\nabla p \cdot \vec{n} = \chi_{11}/\chi_{12}E$) and electroviscosity ($Q/A = -\nabla p \cdot \vec{n}(\chi_{11} - \chi_{12}\chi_{21}/\chi_{22})$) are straightforwardly described as well. The structure of the electrical double layer (EDL) governs the form of the χ_{12} and χ_{21} terms.

For a $z{:}z$ electrolyte in the thin-EDL limit, the four components of the EK coupling matrix are:

$$\chi_{11} \approx r_h^2/8\eta \qquad (9)$$

$$\chi_{12} = -\frac{\varepsilon^* \varepsilon_o}{\eta} \phi_o \qquad (10)$$

$$\chi_{21} = -\frac{\varepsilon^* \varepsilon_o}{\eta} \phi_o \qquad (11)$$

$$\chi_{22} = \sigma_B + \frac{G_s}{r_h} \qquad (12)$$

The χ_{11} term is affected only by the channel size and fluid viscosity; the components off the main diagonal depend on electrical and mechanical properties of the fluid and the wall potential. The χ_{22} term is equal to the system conductivity, composed of bulk conductivity, surface conductance, and the

hydraulic radius of the channel. There are two commonly recognized sources of surface conductance: (1) an electrophoretic component, similar to the bulk, but increased because of enhanced concentration of ions near the surface and (2) a convective component provided by electroosmotic flow, which carries the net charge in the EDL. These two effects were quantified by Bikerman:[31–33]

$$G_s = \sqrt{8\varepsilon^* \varepsilon_o c_\infty RT} \left(\frac{u_+}{B^*-1} - \frac{u_-}{B^*+1} + \frac{4\varepsilon^* \varepsilon_o RT}{\eta z F} \frac{1}{B^{*2}-1} \right) \quad (13)$$

here, $B^* = \coth\left(\frac{-z\phi_o}{4\phi_T}\right)$ and $u_\pm$ are the ionic mobilities of the counter- and coions in solution (cf. Bard and Faulkner[17] p. 68).

We introduce integral formulations of the electrokinetic coupling terms, which generalize the electrokinetic parameters when outside of the thin-EDL limit.[36] Here, the velocity u is a function of both a pressure gradient and electrical potential. Further, the phenomena is reduced to two dimensions – with directions parallel (y) and orthogonal (x) to the flow:

$$\begin{bmatrix} Q/A \\ I/A \end{bmatrix} = \begin{bmatrix} \dfrac{1}{-\frac{\partial p}{\partial y}} \dfrac{1}{\int dx} \int u \Big|_{E=0} dx & \dfrac{1}{E} \dfrac{1}{\int dx} \int u \Big|_{\frac{\partial p}{\partial y}=0} dx \\[12pt] \dfrac{1}{-\frac{\partial p}{\partial y}} \dfrac{1}{\int dx} \int u \Big|_{E=0} \rho_e dx & \dfrac{1}{\int dx} \left(\int \sum_j z_j^* F u_j c_j dx + \dfrac{1}{E} \int u \Big|_{\frac{\partial p}{\partial y}=0} \rho_e dx \right) \end{bmatrix} \begin{bmatrix} -\frac{\partial p}{\partial y} \\ E \end{bmatrix} \quad (14)$$

The quantity u_j denotes the ionic mobility for the jth ion in the system. Representation of this matrix equation in higher dimensions is straightforward, although evaluation of the terms will be complicated by irregularities in geometry. We implement the reduced form above consistent with past work in this field, as well as experimental systems designed to accomodate simplified forms.

2.3 Electrokinetics and soft interfaces

The electrokinetic coupling matrix is a convenient way to codify the response of the diffuse charge system to external forcing. The integral formulation outlines how such responses will be determined, provided that expressions for the fluid velocity and concentrations are known as a function of applied electric and pressure fields both inside and outside of the surface layer.

The generalized electrokinetic coupling terms described in eqn (14) are applicable to soft interfaces. The key difference between rigid and diffuse interfaces with respect to these terms is the breakdown of a well-defined and meaningful ζ-potential. For rigid interfaces, ζ represents the potential at the plane of shear, whereas for soft materials, ζ is an integral function of the soft layer charge and hydrodynamic properties.

2.4 Theoretical descriptions of soft interfaces in electrokinetics

To analyze and interpret theory and experimental data, we use the system geometry in Fig. 2. Here, the height of the channel is small relative to the width ($d \ll w$) and thus the channel geometry can be approximated as infinite parallel plates. A fixed charge

layer of thickness δ uniformly covers each surface. Depending upon the phenomena of interest, pressure or electric fields may actuate the fluid.

Descriptions of electrokinetics at geometrically well-defined soft interfaces have been proposed and studied by many workers. The genesis for the initial work is a description of membrane surfaces, as they appear in filtration systems and biological applications.[37] Although these studies are useful to frame our current discussion on planar interfaces in electrokinetics, we will not discuss results specific to non-planar geometries. Soft systems have also been analyzed with respect to colloidal mobility,[38–40] sharing many aspects of the theory, but these studies are outside of the current discussion owing to the inclusion of complicating factors (e.g., geometry, although this complication vanishes for Debye and diffuse-layer length scales much larger than the characteristic particle size).

Soft interfaces may be divided into two classes: soft interfaces with charge and soft interfaces without charge. Early attempts at modeling the soft interface without charge were provided by Cohen Stuart, et al.[41,42] In their approach, the film completely blocks momentum transfer, yet has electrical properties identical to the bulk fluid. This shifts the shear plane away from the rigid wall into solution by a thickness δ, and is distinct from the Stern layer picture of the interface as the drop within the film layer proceeds exactly as in the bulk, vs. the linear decay demanded by a finite layer of oppositely charged ions. Specifically, Cohen Stuart, et al. assume a solid wall with potential $\phi_o^* = \dfrac{F\phi_o}{RT}$ and a film with thickness δ to obtain the potential at the film edge:
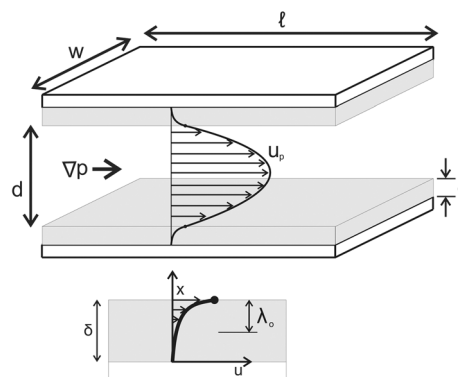

Fig. 2 Schematic of electrokinetic cell used in theoretical modeling and experimental investigations (top). The configuration here is not drawn to scale; typically $w \gg d$ to approximate parallel plates. (Below) a typical velocity profile produced by an applied pressure difference. The hydrodynamic penetration distance, λ_o, is also shown.

$$\phi_\delta = \frac{2RT}{z^*F} \ln\left(\frac{1 + \tanh\left(\frac{\phi_o^*}{4z}\right)e^{-\delta/\lambda_d}}{1 - \tanh\left(\frac{\phi_o^*}{4z}\right)e^{-\delta/\lambda_d}}\right) \qquad (15)$$

For a $z^*{:}z^*$ electrolyte in the case described above, the four components of the electrokinetic coupling matrix are:

$$\chi_{11} = (d/2 - \delta)^2/8\eta \qquad (16)$$

$$\chi_{12} = -\varepsilon^*\varepsilon_o\phi_\delta/\eta \qquad (17)$$

$$\chi_{21} = -\varepsilon^*\varepsilon_o\phi_\delta/\eta \qquad (18)$$

$$\chi_{22} = \sigma_B + \sigma_\delta + \frac{G_s}{d/2 - \delta} \qquad (19)$$

Compared to systems absent the film, the χ_{11} term is affected only by a reduced flow path, and χ_{12} and χ_{21} exhibit reduced electrical potential as the potential drops across the immobile film to the displaced plane of shear. The conductivity term, χ_{22}, now has three components: the bulk conductivity of the channel, σ_B, the conductivity within the stiff film, σ_δ, and a conductivity term accounting for excess and depletion of counter- and coions near the charged surface and an electroosmotic component of the flow, G_s. Here, we take σ_δ to be zero as the film has infinite resistance to flow. Outside the film, we adopt the Bikerman formulation of surface conductivity (eqn (13)). From eqn (16)–(19) we observe that the EK coupling matrix for a transport-impermeable film of thickness δ is nearly identical to a system without a transport impermeable film. The slight differences originate in a decrease in the hydraulic resistance and apparent ζ-potential for the system with a film.

Although the impact of the momentum-impermeable, electrically identical film is straightforward to analyze and interpret, the model can be applied to very few systems: Generally, an interfacial layer will exhibit none of these outcomes – grafted layers are seldom impermeable to transport, and films rarely exist completely uncharged. Indeed, there are many reports of surfaces with no inherent chemical charge generation method[6,25,43,44] (i.e., no dissociable groups or groups that may be substituted) that nevertheless generate a local potential and charge attributable to nonspecific adsorption, or other physical and chemical interactions. Studies of charged interfaces present greater difficulties in analysis and interpretation.

Modeling of soft interfaces is grounded in the examination of biological materials. Early efforts by Donath and Pastushenko[45,46] analyzed the electrophoresis of a cell coated with glycoproteins and glycolipids. The Donath and Pastushenko theory is developed for the linearized Poisson–Boltzmann equation with a uniform fixed charge density in the glycoprotein/lipid layer. Whereas the biological analytes considered by Donath and Pastushenko[45,46] are poorly defined geometrically and heterogeneous in extent, the theory developed assumes planar geometry on the assumption that the characteristic length scale for changes in the electrokinetic and flow profiles are much smaller than the characteristic dimension of the cells under study (erythrocytes and bull spermatocytes).

In the Donath and Pastushenko theory, the inner membrane potential is related to the fixed charge through the Donnan

potential. The concept of the Donnan potential[30,47,48] is central to nearly all studies of diffuse-charge interfaces. A charged membrane will uptake ions from solution, generating a difference in concentration. This is coincident with a difference in potential because the chemical potential of the same species must be equal in both the fluid and film phases.[30] This same relation between bulk fluid and inner membrane potential is obtained from eqn (1) when $d^2\phi/dx^2 = 0$, as a uniform equilibrium is enforced between the salt reservoir and the fixed charge sites. For an ion-permeable membrane with fixed charge density ρ_f and a solution of $z^*{:}z^*$ electrolyte with concentration c_∞ at equilibrium, the Donnan potential is:

$$\phi_D = -\frac{RT}{|z^*|F}\text{arcsinh}\left(\frac{\rho_f}{2|z^*|Fc_\infty}\right) \qquad (20)$$

When the potential and charge density are made dimensionless by ϕ_T and $\beta = 2FI_c$, the Donnan potential becomes:

$$\phi_D^* = -\frac{1}{|z^*|}\text{arcsinh}\left(\rho_f^*\right) \qquad (21)$$

This describes the potential difference between a thick membrane ($\delta \gg \lambda_d$) and a point far out in solution; $\delta \gg \lambda_D$ implies that the curvature in potential will vanish, leaving a balance between the free and fixed charge densities, as above. Ohshima and Ohki[49] require this condition at the interface between the inner and outer layers of the membrane, and this, in conjunction with zero potential gradient at the membrane midline, requires that the center layer of the film assume a potential equal to the Donnan potential. This Neumann boundary condition appears in nearly all descriptions of diffuse-charge interfaces; notable exceptions are those descriptions that select a potential boundary condition deep within the film of the rigid backing substrate (e.g., a boundary potential of silica for a hydrogel attached to glass). This boundary condition is indicated schematically in frame A of Fig. 3.

In the Donath and Pastushenko theory, Donath and Pastushenko[45,46] formulate a three-parameter model varying the thickness of the film, film permeability, and the fixed-charge density of the film. Inherent in their model is the assumption of equal dielectric constant (ε^*) in both the gel layer and solution—an assumption that they assert is justified on the high water content of the film.
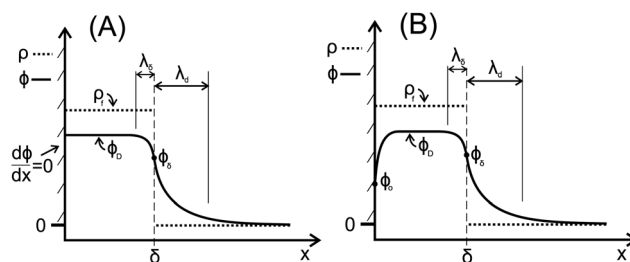

Fig. 3 Diagrams of charge (ρ_f) and potential (ϕ) profiles for various wall boundary conditions. (A): Neumann boundary condition with fixed potential slope at wall. (B): Dirichlet boundary condition with fixed potential at the wall. In both cases, characteristic decay lengths are indicated for the fluid (λ_d) and diffuse charge layers (λ_δ), with ϕ_δ is the electrical potential at the film edge.

Ohshima and Ohki[49] consider the electrical potential profile of a partially charged membrane sandwiched by free solution. In this model, a free membrane in solution has a dry, *uncharged* center and hydrated exterior regions which *are* charged. Their analysis is similar to the prior efforts by Donath and Pastushenko[45,46] although Ohshima and Ohki consider the general nonlinear description of the electrokinetics, and benefit from symmetry conditions at the membrane interior. Considering thin ($2\delta/\lambda_d \sim 1$) and thick ($2\delta/\lambda_d \gg 1$) membranes, they derive an expression relating the potential at the outer plane of the diffuse charge layer with an inner, uncharged, layer that is offset from the outer plane by some distance δ_h. Asserting the uncharged inner layer possesses zero curvature in electrical potential ($d^2\phi/dx^2 = 0$), and defining the center of the membrane as a plane of symmetry $\left(\frac{d\phi}{dx}\Big|_{midpoint} = 0\right)$, they relate the potential at the outer membrane boundary to points within the inner layer of the membrane:[49,50]

$$\phi_\delta^* = \phi_D^* - \tanh(\phi_D^*/2) \tag{22}$$

here, ϕ_δ^* lies on the edge of the membrane/film and ϕ_D^* lies in the plane dividing the charged and uncharged membrane sections; ϕ_D^* is also the potential everywhere *within* the uncharged membrane; both potentials are made dimensionless by ϕ_T (Fig. 4).

2.5 Charge transport: χ_{12} and χ_{21}

Studies of electrokinetic behavior on diffuse-charge interfaces have been conducted for planar (or nearly planar) surfaces by Wunderlich,[51] Donath and Voigt,[52] Ohshima and Kondo,[53] and Starov and Solomentsev.[54,55] Donath and Voigt[52] compute the streaming current and streaming potential of diffuse-charge
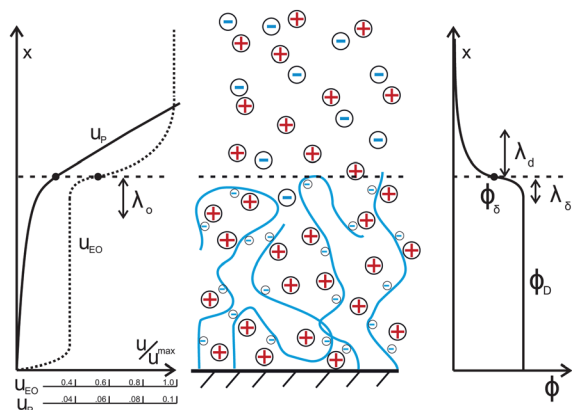

Fig. 4 Schematic of potential and velocity profiles for a negatively charged polymer film. Various momentum and potential decay scales are displayed, which mitigate both pressure and electric field actuated transport. In the velocity–position plot at left, the u_p and u_{EO} plots are not comparable in magnitude, but do indicate differences in spatial velocity gradients; pressure-driven flow changes continuously until the channel center, and local to the film varies linearly when the size of the channel is large as compared to the film thickness. The E-field generated (electroosmotic) flow establishes on scales comparable to the Debye length.

layers on parallel plates. Their formulation of the system includes fluid mechanical and electrical modeling. They solve a modified Navier–Stokes equation by including a Brinkman-type[56] resistance term:

$$\eta\frac{d^2u}{dx^2} - k(x)u = \frac{\partial p}{\partial y} \tag{23}$$

which we nondimensionalize to:

$$\frac{d^2u^*}{dx^{*2}} - \lambda^{*2}u^* = \frac{\partial p^*}{\partial y^*} \tag{24}$$

where $u^* = u/U$ defines a characteristic velocity scale U, $y^* = y/\ell$ and $x^* = x/\delta$ define length scales based on channel length and film thickness, the pressure is nondimensionalized as $p^* = \frac{p}{\eta\ell U/\delta^2}$, and $\lambda^* = \sqrt{\frac{k(x)\delta^2}{\eta}}$ defines the square of the ratio of a characteristic length scale for the penetration of fluid into the film, $\lambda_o = \sqrt{\frac{\eta}{k(x)}}$, which nondimensionalizes the film thickness, δ. The Brinkman (friction) coefficient, $k(x)$, is a function of space and may generally be taken to vary in direct proportion to the charge density of the film, as the density of charge groups on the polymer is presumed to scale linearly with the film volume fraction and hence film resistance. In the Donath and Voigt formulation, the friction coefficient is non-zero and uniform throughout the film $0 \leq x \leq \delta$, and zero in the pure fluid phase $\delta \leq x \leq d/2$.

The electrical modeling of the planar fixed-charge layer and fluid assumes the form given by eqn (1), with a spatially varying fixed-charge density ρ_f. Studying the cases of a $z^*:z^*$ electrolyte, the problem is then to solve eqn (2), with $\beta = 2FI_c$. Since the full equation is nonlinear, most closed-form solutions have been found only for the linearized case. Linearization results in:

$$d^2\phi^*/dx^{*2} = -\phi^* + \rho_f^*(x) \tag{25}$$

This now limits the applicable range of study to cases where $\phi^* < 1$ or equivalently $\phi < 25$ [mV]. Eqn (25) may be solved both inside and outside of the film, applying a matching condition for electrical potential and electrical field at the film edge. The boundary conditions away from the film are zero potential in the bulk (cell midline) and fixed potential slope at the inner surface of the film:

$$\phi^*(d/2\delta) = 0 \tag{26}$$

$$\frac{d\phi^*}{dx^*}\Big|_{x^*=0} = -\sigma^* \tag{27}$$

here, $\sigma^* = \frac{\sigma}{\sqrt{2\varepsilon\varepsilon_o RTI_c}}$. The first condition enforces electroneutrality of bulk solution, and the second fixes the charge of the film interior to that of the bulk film, neglecting any apparent charge at the solid wall that would result from, for example, a charge-generating dissociation reaction. Both of these boundary conditions are indicated in Fig. 3.

The distribution of fixed charge within the film strongly affects the film surface potential and surface-sensitive measurements. In Fig. 5 we plot analytical solutions to eqn (25) with various charge density profiles, all having the same total charge. These profiles
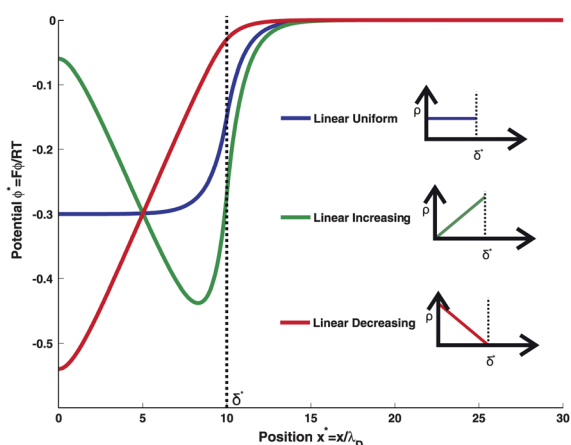
Fig. 5 Potential profiles for various charge distributions derived from eqn (25). The film extends a distance $10\lambda_d$ into the domain from the wall ($x^* = 0$). The inset figures (at right) show the various charge distributions, ρ, considered. In all cases, the total charge is conserved across the film of thickness δ^*.

indicate the dependence of profile shape and boundary value on the charge distribution. Considering the effect of charge distribution on film measurements, streaming current preferentially probes the surface of the film, and is sensitive to the charge density at the surface (as determined by the potential). The surface potential varies strongly in for the three charge distributions considered.

Donath and Voigt[52] examine streaming current as a function of system parameters in the low potential limit. These results do not address films having high charge or films bounded by surfaces with electrical boundary conditions that differ from the film boundary conditions. Donath and Voigt[52] also describe a nonlinear treatment of streaming current, streaming potential, and surface conductivity for a volume with uniform charge distribution terminated by a surface with fixed surface charge. A numerical approach was required to produce a solution to the problem of ion transport under the action of pressure and electrical fields.

The identical problem was considered by Ohshima and Kondo,[53,57] who additionally show in the limits $\delta/\lambda_d \gg 1$ and $\delta/\lambda_o \gg 1$ that Onsager reciprocity is satisfied in the system (*i.e.*, $\chi_{12} = \chi_{21}$). In this case, the fixed charge density is distributed uniformly across a distance δ from the wall into the fluid. A closed-form solution is available for the off-diagonal term of the EK coupling matrix:

$$\frac{\chi_{12}}{\mu} = \frac{\chi_{21}}{\mu} = \frac{\lambda^*\phi_\delta^* + \phi_D^*\delta^*\cosh^{1/2}(^*z\phi_D^*)}{\lambda^* + \delta^*\cosh^{1/2}(z^*\phi_D^*)} + \rho_f^*\left(\frac{\delta^*}{\lambda^*}\right)^2 \quad (28)$$

Here, the potentials ϕ_δ^*, and ϕ_D^* are uniquely determined by the film charge ρ_f^*; ϕ_D is given by eqn (21), and ϕ_δ^* has been derived in eqn (22). We introduce a scale for the streaming current term, as suggested by eqn (10), $\mu \sim \dfrac{\varepsilon^*\varepsilon_o RT}{\eta F}$; this is equivalent to the electroosmotic or electrophoretic mobility of a wall or particle having a surface potential equal to the thermal voltage. The χ_{12} and χ_{21} terms are a function of the charge density in the film, as well as the parameters λ^* and δ^*.

Extensions and considerations beyond the models of Donath and Voight[52] and Ohshima and Kondo[48,53,57] have been made in recent studies. In a pair of papers, Starov and Solomentsev describe the effects of diffusion[54] in the film and consider the interaction between ions in the fluid and the film to develop an apparent electrokinetic potential.[55]

Theoretical determinations of surface conductivity have also been considered by Ohshima and Kondo[53] and Donath and Voigt.[52] Ohshima and Kondo[53] describe χ_{22} in terms of the bulk conductivity only, whereas Donath and Voigt[52] describe enhancements of conductivity due to the presence of the film layer (concentration enhancement/depletion as well as electroosmotic effects), although their expression requires knowledge of ϕ_δ^*, which is only known explicitly in specific cases, as discussed by Ohshima and Kondo.[53]

The terminating geometry of the adhered film is an important film characteristic, determining both the distribution of fixed charge and the local resistance of the polymer network. Duval and van Leeuwen[58] and Duval[59] pose and examine a distribution of uniform fixed charge that terminates into solution with a linear decay. Their models suppose a film friction that varies proportionately with the fixed charge density profile. Later, a smooth hyperbolic function was used to describe the transition from finite to zero fixed charge.[60]

Duval and van Leeuwen[58,59] solve the piecewise-charged film with both linear[58] and nonlinear[59] analyses. In both cases, the parameters δ, λ_o, and the characteristic dimension of the film transition α, are essential in the EK description of the film–fluid system. They obtain solutions to the hydrodynamic and electrical profiles in solution, analyze the streaming current produced by an imposed pressure gradient, as well as current produced by a transverse electric field. The piecewise nature of the fixed-charge profile leads to a complicated expressions for the streaming current within the system, we omit this expression here.

The linear Duval and van Leeuwen model[58] illustrates the interplay between momentum and potential profile decay from regions of high charge density and low velocity to low charge density and high velocity: films with $\alpha/\lambda_d \gg 1$ exhibit *lower* values of streaming potential because of decreases in fluid velocity where a net charge exists – at a flat interface, the decay of electrical potential occurs in the free fluid, whereas a film with a gradual linear decay of charge into solution has simultaneous screening of charge and momentum. For $\alpha/\lambda_d \ll 1$, the electrical potential dissipates within the region of retarded flow, reducing the net charge convected by the fluid. The linear model presented by Duval and van Leeuwen is restricted to cases where $\delta^* \gg 1$, and $\phi_D^* < 1$.

In describing the potential profile and charge transport due to the presence of a soft layer, we remark that many studies do not account for the charge of the bare solid surface when formulating expressions for charge transport. It is only correct to neglect the influence of the solid potential boundary condition when the film is sufficiently thick as compared both to the hydrodynamic penetration length of the film, $1/\lambda_o$, and the Debye length of the fluid. In the case of a $\delta \gg 1/\lambda_o$ and λ_d for a film probed with pressure driven flow, charge transport is nearly extinguished near the wall while charge at the outer surface of the membrane is easily convected. If the film is *thin* as compared to $1/\lambda_o$ and λ_d, then the wall potential must be accounted for. Such relations can be derived in the limit of low electrical potentials (Debye–Huckel

limit) and numerical simulation is generally required for arbitrary potentials.

Duval used a numerical solution to extend their linear analysis of charged films[59] to the general nonlinear, unrestricted ϕ_D, case with the same geometry. The scaling of the Donnan potential (cf., (21)) implies that the nonlinear theory will be applicable at low solution ion concentration, as large concentrations drive the film–solution equilibrium toward low values of interfacial potential difference ($\Delta\phi = \phi_D - \phi(\infty) \ll 1$). The disparity in streaming potential between the linearized and nonlinear theories is most apparent at low solution concentration and low λ_o/λ_d (cf. Duval[59] Fig. 7).

In the Duval and van Leeuwen[58,59] and subsequently considered models, film hydrodynamics are described with a Brinkman-modified Navier–Stokes eqn (23). This approach follows Brinkman,[56] who proposed a Stokes-like equation to describe the motion of fluid within a dense collection of particles. Debye and Bueche[61] derived a resistance expression applicable to polymer films by assuming the polymer may be described as a string of Stokeslets, with each Stokeslet along the string acting as a resistance center. The Brinkman approach is implemented for flows in porous-media, and descriptions of porous media hydrodynamics are available in the monographs by Scheidegger[62] and Happel and Brenner.[63] As observed by Dukhin et al.,[64] the Brinkman–Debye–Bueche approach is widely used in the description of soft polymer layers. In many cases, the mechanical attributes of the diffuse layer are assumed, assigned, or varied to demonstrate trends in the behavior of the proposed theories.[38,41,45,46,65,66] In others, such as Duval and van Leeuwen[58,59] the Debye and Bueche approach[61] is used to correlate the local resistance and local charge of the film, because of the assumption that regions of higher polymer density contain higher charge.

The Debye–Bueche approach leads to a direct expression for the Brinkman friction term. The dimensional resistance is written as:[58]

$$\frac{\lambda^*}{\delta} = \sqrt{\frac{k(x)}{\eta}} = \left(\frac{R^2}{18} \left(3 + \frac{4}{\varphi^*(x) - 3\left(\frac{8}{\varphi^*(x)} - 3\right)^{1/2}} \right) \right)^{-1/2}$$

(29)

With R the characteristic radius of a spherical polymer segment, and $\varphi(x)$ the volume fraction of polymer in the fluid–film system; for $\varphi^*(x) \ll 1$, $\lambda^*/\delta \approx 6/R + \varphi^{*1/2}(x)/(3\sqrt{3}R) + O(\varphi^*)\dots$. Experimental investigations on diffuse charge interfaces (discussion below) typically implement this description for polymer layers with low volume fraction of solids. Duval and van Leeuwen[58] cite a limit of $\varphi^*(x) < 0.6$ for the above expression (and themselves apply it in a dilute limit, $\varphi^*(x) < 0.05$), although a Stokesian dynamics analysis of the Brinkman equation by Durlofsky and Brady[67] places further limits on this technique, determining that the Brinkman formulation of the system mechanics is applicable only in the limit of dilute solids, $\varphi^*(x) < 0.05$.

2.6. Film and fluid conductivity: χ_{22}

With three of the four electrokinetic coupling matrix components already having been discussed, we now turn to χ_{22}. The χ_{11} term

describes the impact of the film on the hydraulic resistance of the flow; for systems with $\delta \ll d/2$, this effect is minimal. The χ_{12} and χ_{21} terms (closed form in specific limits) describe the response of flow and current to lengthwise electrical potential and pressure gradients, respectively; here, the impact of the fixed charge layer depends non-trivially on the charge distribution and density, ion concentration, film thickness, δ^*, and film hydrodynamics, λ^*. The final term χ_{22} relates current to the electric field, E, and is considered presently.

The presence of a surface locally affects the conductivity of a fluid. The standard Bikerman model[31–34] of surface conductivity accounts for the enhancement and depletion of ions in a field-induced convection of counterions and coions produced by a surface charge, as well as the electroosmotic transport of ions produced by actuation of the carrier fluid; both of these phenomena are necessarily actuated by a transverse field gradient E. These same transport processes occur within the soft diffuse-charge layer attached to a rigid surface. Given a precise enough model for these processes, conductance measurements combined with physicochemical measurements of the film and solution provide sufficient information to characterize the electrokinetic potentials of the system. Streaming potential measurements also require the system conductivity, although only the measured value is required to interpret streaming potential data; analytical expressions are not needed for measurements.

The total conductivity is separated into contributions from the surface (charged film and adjacent layer with net charge) and bulk (no net charge). The conductivity is additive in bulk and surface conductivities:

$$\chi_{22} = \sigma_B + \sigma_s$$

(30)

It is customary to separate the surface conductivity term into ionic and electroosmotic conductances, along with a length scale, r_h:

$$\sigma_s = \frac{1}{r_h}(G_I + G_{EO})$$

(31)

For the systems we are examining here, we further decompose each component into parts interior and exterior to the charged layer:

$$G_I = G_{I,i} + G_{I,o}$$

(32)

$$G_{EO} = G_{EO,i} + G_{EO,o}$$

(33)

Given a film over $0 \leq x \leq \delta$ the ionic component is:

$$G_I = 2F \sum_j \left| z_j^* \right| u_j \int_0^{d/2} (c_j(x) - c_{j,\infty}) \mathrm{d}x$$

(34)

$$G_{I,i} = 2F \sum_j \left| z_j^* \right| u_j \int_0^{\delta} (c_j(x) - c_{j,\infty}) \mathrm{d}x$$

(35)

$$G_{I,o} = 2F \sum_j \left| z_j^* \right| u_j \int_\delta^{d/2} (c_j(x) - c_{j,\infty}) \mathrm{d}x$$

(36)

here the sum, j, is over all ions in the layer, and u_j denotes the ionic mobility of the jth ion. Similarly for the electroosmotic conductance:

$$G_{\text{EO}} = \frac{2}{E} \int_0^{d/2} u(x) \bigg|_{\frac{\partial p}{\partial y} = 0} \rho_e(x) \mathrm{d}x \qquad (37)$$

$$G_{\text{EO,i}} = \frac{2}{E} \int_0^{\delta} u(x) \bigg|_{\frac{\partial p}{\partial y} = 0} \rho_e(x) \mathrm{d}x \qquad (38)$$

$$G_{\text{EO,o}} = \frac{2}{E} \int_\delta^{d/2} u(x) \bigg|_{\frac{\partial p}{\partial y} = 0} \rho_e(x) \mathrm{d}x \qquad (39)$$

Analytical expressions for conductivity are generally available only in systems with thin or thick films with simply specified charge and fluids.

We write a representation for the χ_{22} term, following the work of Dukhin, *et al.* Several other workers have also presented analytical expressions where available, and have performed numerical analyses when closed-form expressions are unavailable. Donath and Voigt[52] consider the case of a uniform charge distribution producing a uniform potential within the charged layer. Duval and van Leeuwen examine surface conductivity in both the linear case[58] with an analytical theory, and the nonlinear case[59] implementing numerical methods for a film with a linear transition from the charged layer to zero charge in solution. Dukhin, *et al.*[18] relate measurements of surface conductivity to charge and potential characteristics of polyelectrolyte films with a uniform distribution of pH sensitive charged sites.

We describe here the Dukhin, *et al.* approach for anionic or cationic films that charge as a function of the proton concentration (pH). Supposing an anionic polymer film with a proton dissociation reaction $HA \rightleftharpoons H^+ + A^-$ and the negative logarithm of the acid dissociation constant pK_a, the following charge–pH relation results:

$$\rho_f^*(x) = \frac{\rho_f^{*\max}}{1 + 10^{pK_a - pH} e^{-\phi^*(x)}} \qquad (40)$$

Here, $\rho_f^{*\max}$ is the charge density of acidic groups (with concentration A^-) and is equivalent to $A^-/(2I_c)$ at full dissociation. The fraction of dissociated groups is dependent upon the local pH surrounding the charged site – a potential biases the concentration of hydronium ions, modifying the concentration from the bulk value in solution. This dissociation approach was first discussed by Donath and Voigt.[52] The Donnan potential is calculated as described previously – by combining eqn (20) with the curvature-free form of the Poisson–Boltzmann equation. For the case of a 1 : 1 electrolyte, eqn (40) becomes:[18,68]

$$\sinh(\phi_D^*) = \frac{-\rho_f^{*\max}}{1 + 10^{pK_a - pH} e^{-\phi_D^*}} \qquad (41)$$

The Donnan potential must necessarily be determined numerically in this form. When coions are excluded within the film, Dukhin, *et al.*[18,68] have derived an expression for the Donnan potential:

$$e^{-\phi_D^*} = \frac{10^{pH - pK_a}}{2} \left(\sqrt{1 + 8 \left| \rho_f^{*\max} \right| 10^{pK_a - pH}} - 1 \right) \qquad (42)$$

Dukhin *et al.* further derives a result analogous to the Ohshima and Okhi relation between the Donnan and surface potentials of a thick film (*cf.*, eqn (22)):

$$\phi_D^* - \phi_\delta^* + \ln\left(\frac{1 + 10^{pK_a - pH} e^{-\phi_D^*}}{1 + 10^{pK_a - pH} e^{-\phi_\delta^*}} \right)$$
$$= \tanh\left(\frac{\phi_D^*}{2} \right) \left(1 + 10^{pK_a - pH} e^{-\phi_D^*} \right) \qquad (43)$$

The surface and Donnan potentials are explicitly related when the film charge is independent of pH, or when the film is fully dissociated. When the film charge is pH dependent and not fully dissociated, eqn (43) must be solved in a limit of high or low dissociation, where an implicit relationship between ϕ_D^* and ϕ_δ^* has been obtained. For nearly complete dissociation (*i.e.*, high pH):

$$\phi_\delta^* - \phi_D^* = \ln\left(\frac{e^{s^*} + s^* - 1}{s^*} \right) \qquad (44)$$

For small amounts of dissociation (*i.e.*, acidic groups at low pH):

$$\phi_\delta^* - \phi_D^* = \ln(2 + s^*) \qquad (45)$$

In both these relationships, $s^{*-1} = 1 + 10^{-pH\left(1 - \frac{pK_a}{pH}\right)} e^{-\phi_D^*}$, which represents the degree of dissociation in the film – for eqn (44), $s^* \sim 1$ and for eqn (45) $s^* \ll 1$.

The surface conductance is then obtained with the assumption that the Donnan potential describes the potential everywhere within the film, which is valid when $\lambda_\delta/\delta \ll 1$. The approach is to use eqn (35) and (36) with $c_i(x) = c_{i,\infty} e^{-z_i \phi_D^*}$ in the film and $c_i(x) = c_{i,\infty} e^{-z_i \phi^*(x)}$ in the diffuse layer, where $\phi^*(x)$ solves the Poisson–Boltzmann equation outside the film given the boundary condition ϕ_δ^* at the film edge, and a potential of zero in solution. In both these cases, the solution is known – the integrals vanish inside the film, and outside the film we use the Bikerman expression for the diffuse component side:[18]

$$G_{\text{I,i}} = 2F \sum_j \int_0^\delta \left| z_j^* \right| u_j c_{j,\infty} \left(e^{-z_j^* \phi_D^*} - 1 \right) \mathrm{d}x$$
$$= 2|z^*| F \delta c_\infty \left(u^+ \left(e^{-z^* \phi_D^*} - 1 \right) + u^- \left(e^{z^* \phi_D^*} - 1 \right) \right) \qquad (46)$$

$$G_{\text{I,o}} = 2F \sum_j \left| z_j^* \right| u_j \int_0^{d/2} \left(c_j(x) - c_{j,\infty} \right) \mathrm{d}x$$
$$= 2|z^*| F \lambda_d c_\infty \left(u^+ \left(e^{-z^* \frac{\phi_\delta^*}{2}} - 1 \right) + u^- \left(e^{z^* \frac{\phi_\delta^*}{2}} - 1 \right) \right) \qquad (47)$$

Eqn (46) and (47), are written for a $z^*:z^*$ electrolyte. Furthermore, supposing a film excluding coions, the conductance is further simplified, as the migratory conductance within the film depends completely on the counterionic species as:[18]

$$G_{\text{I,i}} = \frac{\sigma_B \delta}{2} e^{-\phi_D^*} \qquad (48)$$

where $\sigma_B = 2F c_\infty u^+$ is the bulk conductivity in the same limit of ion exclusion.

Dukhin, *et al.*,[18] following Ohshima,[69] examine the relative importance of electroosmotic and migratory components of the surface conductivity, assuming a model for electroosmosis within the film where the electrical body force balances fluid and film-induced friction within the diffuse charge layer. Their model is written as:

$$\rho_e E - k u_{EO} = 0 \tag{49}$$

where k is, again, the volumetric frictional force constant retarding the convected charge by the polymer film. This limiting form of transport within the film is obtained by examination of the Navier–Stokes–Brinkman equation with zero pressure gradient and nonzero electric field forcing and charge density, $\rho_e E + \eta \nabla^2 u - ku = 0$. Taking the scales $\nabla^{*2} = \delta^2 \nabla^2$, $u = u^* \frac{\varepsilon\varepsilon_o \phi_D}{\eta} E$, $\rho_e = \rho_e^* 2FI_c$, $\phi_D = \phi_D^* \frac{RT}{F}$, and assuming a fully dissociated film with a 1 : 1 electrolyte ($\phi_D^* = -\mathrm{arcsinh}(\rho_e^*)$), the nondimensional form is $\left(\frac{\delta}{\lambda_d}\right)^2 \frac{\sinh(\phi_D^*)}{\phi_D^*} - \nabla^{*2} u^* + \lambda^{*2} u^* = 0$. For a thick ($\delta/\lambda_d \gg 1$), highly resistive film ($\lambda^* \gg 1$), the $\nabla^{*2} u^*$ term is small and the balance is between charge forcing and volumetric film friction.

The limit of the in-line momentum balance leading to eqn (49) is not unique, but is consistent given the limits in which the momentum balance is applied. Two other velocity scales yield additional balances: $U \sim 2FI_c E\delta^2/\eta$, which is a viscous scaling for velocity, and $U \sim 2FI_c E/k$, which is a Brinkman balance. The viscous balance yields $\rho_e^* + \nabla^{*2} u^* - \lambda^{*2} u^* = 0$. For $\lambda^* \gg 1$ this implies a boundary-condition-contradictory velocity that is additionally independent of charge–potential forcing; neither of these implications is necessarily the case for a resistive film. The Brinkman balance gives $\lambda^{*2} \rho_e^* + \nabla^{*2} u^* - \lambda^{*2} u^* = 0$, which limits to eqn (49), as expected given the assumed velocity scale. Synthesizing these limits, the Smoluchowski scale is valid for thick films where $\delta \gg \lambda_o \sim \lambda_d$, implying that the interface appears as rigid to the bulk flow. The viscous balance is untenable for descriptions of field-forced flow ions within the film, and the Brinkman balance satisfies physical intuition for flow behavior in the film.

Enhanced friction within the diffuse charge layer relegates the electroosmotic component of the surface conductance to a minor role. Extending the analysis introduced previously (eqn (49)), Dukhin *et al.*[18] show that the electroosmotic component of surface conductivity is minimal both in and outside of the film when $\delta \gg \lambda_d$, $\delta \gg \lambda_\delta$, and $\lambda \gg 1$. In a later work, Dukhin *et al.*[70] examine effects of diffuse-layer conductance in a film with a variable charge density. In this analysis, the central simplification is a spatially varying interior film potential that matches exactly with the local Donnan potential of the film (derived by the local charge density). Dukhin *et al.*[70] require that the characteristic length over which charge density variations occur in the film, λ_e, be large as compared to the characteristic electrical decay length in the charged film:

$$\frac{\lambda_e}{\sqrt{2}\lambda_d} e^{-1/2\phi_D^*} \geq 3 \tag{50}$$

For slowly varying charge densities with no coions, Dukhin *et al.*[70] discuss procedures to measure the thickness and charge density for fully and partially dissociated films. These approaches

require knowledge of the chemistry of the film combined with streaming current measurements at varying states of film dissociation (*i.e.*, pH).

2.7 Film property variation

Although the discussion in the previous section has presumed that solution properties inside and outside of the fixed-charge layer are identical, we must in general consider that the properties within the fixed charge layer can differ from those in the bulk solution. We have tacitly assumed that the conductivity of the electrolyte acts independently of the volume fraction of the film – that the only effect of the film on the migratory component of the ions in solution lies in the change in local concentration of the ions introduced by fixed charges in the film. Any additional resistance from the space-filling nature of the gel has been neglected in our presentation. Several authors have discussed the effects of diminished conductivity due to the presence of the polymer network.[18,70–73] The enhanced conductance is related to diffusion, as the two are linked *via* the mobility of the ions through the Nernst–Einstein equation and Kohlrausch's law.[17] The results discussed here apply to charge carriers small as compared to the microscopic dimensions of the film – typically ions such as Cl^-, Na^+, and the like. Larger molecules, such as proteins or DNA, also feel diminished diffusion, but such theories are not considered here.

Most of the theories, however, exhibit agreement with experiment only at small polymer volume fraction. Masaro and Zhu[74] review many theories for diffusion of species, such as proteins or other polymers, in dilute to concentrated polymer solutions. The first-order correction to the bulk conductivity (or mobility) of ionic species caused by the polymer as presented by Dukhin *et al.*[18,70] is:

$$\sigma_p/\sigma_B = 1 - G^* \varphi^* \tag{51}$$

Expressions of this form, in the limit of low concentrations, appear in many theoretical formulations of retarded diffusion (D), electrophoretic (E) and sedimentation (S) measurements. Odijk[75] cites the form of an experimental fitting curve:

$$\frac{E}{E_o} = \frac{D}{D_o} = \frac{S}{S_o} = F^* = e^{K_r a^{\mu^*} c_p^{\nu^*}} \tag{52}$$

where the subscript naught denotes the transport process (diffusion/electrophoresis/sedimentation) of an object with characteristic radius a in free solution; quantities above (E,D,S) represent the same transport processes in a solution with polymer concentration c_p. Here, the constants K_r, μ^*, and ν^* are determined experimentally by a fit of experimental data to the exponential function; several representative values of these parameters are available in Table 1 of Odijk,[75] specifically, for the semi-dilute regime. Typical values for ν^* and μ^* are between 0.5 and 1, with a skew toward unity. The small-argument limit of the fitting relation becomes $F^* \sim 1 - K_r a^{\mu^*} c_p^{\nu^*} \sim 1 - G^* \varphi^*$, consistent with the formula used by Dukhin *et al.*;[18,70] G^* is a term of lumped model parameters to stress the scaling of volume fraction.

Several theoretical expressions have the form of eqn (52), notably a Cukier model accounting for hydrodynamic

corrections to the diffusion of Brownian spheres within a polymeric solution.[74–76] In the development of a model for Brownian spheres, Cukier[76] expounds a theory corresponding to a Debye–Bueche type network of entangled polymer. This model describes a collection of Brownian spheres interacting with a series of deformable pearl strings:

$$\frac{D}{D_o} = e^{-\sqrt{\frac{fn_p}{\eta}}R} \sim 1 - G^*\varphi^{*1/2} \tag{53}$$

where the additional variables f and n_p are the monomer friction factor and the number density of polymer segments. Another scaling for the same regime of polymer concentration suggested by de Gennes[75,77] assumes the form:

$$D/D_o = e^{R/\xi} \sim 1 - G^*\varphi^{*3/4} \tag{54}$$

where $\xi \sim c_p^{-3/4}$ is the correlation distance of the polymer in solution, which represents the length over which the polymers begin to strongly interact. The review by Masaro and Zhu[74] provides a summary of proposed scalings of concentration with the correlation length, and note that despite theoretical and experimental determinations of this value (between 0.5 and 1); consensus has yet to be reached.

Inhomogeneity in the dielectric constant between the pure fluid and fluid–film phases has been discussed briefly by several researchers.[48,49,54,55] The dielectric constant of water is known to vary in response to strong electric fields[78,79] ($d\phi/dx \gtrsim 10^9$ [V m^{-1}]), although generation of a field large enough is unlikely, and, for the purposes of the model, would only occur in thin regions near the boundary of the film. Finer descriptions of the polymer microstructure would be necessary to discern any impact of local fields on the dielectric constant of water, as is done with polymers for proton exchange in energy applications.[80] In addition to the field strength, the dielectric constant of water is affected by the local concentration of ions. This effect is communicated in the low-concentration limit by the dielectric increment[19,79] $d\varepsilon/dc_i$, affecting ε to first order in concentration: $\frac{\varepsilon^*(c_1, ..., c_n)}{\varepsilon_o} = 1 + \sum_{i=1}^n c_i \frac{d\varepsilon^*}{dc_i}$. Here, c_i is the local ion concentration. Investigations of diffuse charge interfaces accounting for the high-field and dielectric increment variation on the dielectric constant have not been found in the literature in the context of electrokinetics.

Changes in bulk mobility (or diffusion) and dielectric constant within the film illustrate uncertainties that may arise when attempting to interpret experimental conductivity data. Other sources of uncertainty within polymer films not captured by the analytical theory include solid-boundary effects in which the potential at the interface between the film and the solid wall differs from the Donnan potential of the film (i.e., $d\phi/dx \neq 0$), and instead assumes some potential determined by rigid surface and solution chemistry. Similar analytical approaches as discussed previously may be implemented for small wall potential (e.g., via linearized Poisson–Boltzmann equation) and films that exhibit a region of zero curvature, essentially insulating the nonuniform potential regions on either end of the film; this is similar in some respects to the sandwiched membrane description of Ohshima and Ohki.[49] Computational approaches are necessary to determine

potentials in systems in which the film is thin compared with the Debye length ($\delta/\lambda_d \lesssim 1$), the Donnan potential of the film is large ($\phi_D^* \gtrsim 1$), or the charge density within the film is nonuniform. Such an approach was taken by Duval[59] to examine a nonuniform diffuse charge interface with a large Donnan potential.

3 Experiments

Depending on the theory to be tested and the information desired, a variety of techniques are available to validate soft diffuse-charge interface theory and determine precisely the surface properties of natural and synthetic systems. Many of these techniques were mentioned in the introduction; we focus here on streaming potential and streaming current techniques, along with conductance measurements for these systems. As was discussed in the theory section, an understanding of surface conductance in diffuse charge systems is necessary to move from measurements of streaming current to streaming potential, or to gain information on film properties directly from a conductance measurement when system conductances are unknown. Furthermore, membrane orientation relative to the direction of flow affects measurement outcomes, and must be considered when interpreting experimental data.

We are concerned with surface measurements in which the flow is along the surface of the diffuse charge interface. When combined with the theory outlined previously, these measurements provide information on the Donnan (ϕ_D) and surface (ϕ_δ) potentials of the film. When supplemented by physical and chemical properties of the film (such as film thickness or film charge density), the theories can be tested more rigorously to determine their range of applicability and precision.

Although we have focused in previous sections on film–fluid systems in which the flow direction is perpendicular to the surface normal of the film, many studies have been performed with flow parallel to the surface normal. The parallel technique has a historical pedigree,[29] having been used for the determination of electrokinetic potentials of inorganic materials in plug form. This porous plug technique limits to the standard electrokinetic behavior on hard surfaces when the interstices among the packed particles (i.e., the pores of the porous plug) are large relative to λ_d. For polymeric materials, the characteristic flow size in the polymer is poorly defined, and is unlikely to be everywhere large relative to λ_d. Additionally, through-membrane as opposed to over-membrane techniques fail to probe the diffuse layer at the film–fluid interface. Through-membrane techniques do, however, fully probe the inner structure of the membrane (e.g., ϕ_D via conductivity measurements), and may supplement over-membrane measurements if the structure of the membrane is isotropic in both measurement modes. Through-membrane analysis is well suited to filtration, ion-exchange, or proton conducting membranes[81–86] because the quantity of interest is often the streaming potential coefficient $\Delta V/\Delta P$ rather than a parameter such as ϕ_D or ζ; this distinction is important, as the through-membrane experiments usually result in measurements of a engineering constant only whereas over membrane measurements, when coupled with the theory, can lead to physical material/solution properties.

Streaming current, streaming potential, and conductance measurements must, in general, be taken at multiple solution and

film states. In a given electrokinetic experiment, the maximum film charge density, degree of dissociation, film chemistry, and film thickness are generally not known *a priori*. These quantities are required to predict all electrokinetic phenomena. The degree of dissociation and film thickness are properties of solution pH and ionic strength, so electrokinetic determination of film thickness and charge will, in general, require more than two measurements and will typically be done over a range of pH and ionic strength. In some cases, auxiliary measurements, such as film thickness with an ellipsometer, or film charge by potentiometric titration, are performed to further inform the film state. Conductivity measurements provide information on the bulk film state (ϕ_D), and require film dissociation, thickness, and ion mobility information corresponding to each measurement. When these parameters are not measured at each point, a parametric model predicting these values over the experimental range of ionic strength and pH is required.

Several workers have performed conductivity measurements to directly examine charged films. Yezek[87] performed conductivity measurements on polyacrylamide-*co*-sodium acrylate gels of varying polymer volume fraction over a range of ionic strength at a pH of 5.8, corresponding to the natural pH of the polymer–solution mixture. In this work, both full- and partial-dissociation models are used to examine the charge density developed in the gel, with the pK_a-dependent dissociation model predicting the observed ratio between the bulk and total conductivities. Theoretical predictions of surface conductivity match the experimental data in the limit of high ionic strength. At lower ionic strengths (less than 1 mM), the full dissociation model diverges from both the partial dissociation theory and experiment. A similar approach was used in a prior work by Yezek and van Leeuwen[88] where, in addition to conductivity measurements, streaming potential and potentiometric titration measurements were conducted. There, conductivity measurements and potentiometric charge measurements yielded agreeable Donnan potential values over the range of ionic strength tested. Streaming potential measurements, however, failed to predict quantitatively the observed zeta potential. In their streaming potential model, Yezek and van Leeuwen[88] implemented a modified Smoluchowski formula accounting for the additional conductance introduced by the film, but did not account for other transport characteristics in the film. An interesting artifact of both of these studies[87,88] is the ratio of cell and bulk conductivities at high ionic strength. This artifact of the experimental limits was examined by Yezek[87] and Dukhin et al.;[18] as the ionic strength increases, ϕ_D decreases, $\phi_D \sim q_f/Fc_\infty$, relegating electrokinetic surface conductivity effects to minor roles. The small difference in conductivity is then ascribed to the blocking effects of the polymeric network. This limit of ionic strength can inform experimentalists on the behavior of hindered conductance measurements in polymeric materials. Freudenberg et al.[89] executed a similar study, performing streaming current, conductance, and ellipsometry studies on crosslinked and uncrosslinked cellulose films. Here, thick-film theory was used to determine ϕ_D within the film from the surface conductivity of the film layer, as determined by the ratio of streaming current and streaming potential measurements, knowing precisely the geometry of the flow cell. The measurements revealed electrokinetic variance in the film between crosslinked and uncrosslinked

states, with strong dependence of film conductance on crosslinking state (lower upon crosslinking), and small differences in Donnan potential.

Although the discussed works[87–89] have analyzed the system by assuming a uniformly distributed charge within the film, and a bounding rigid surface having no affect on the film charge distribution or potential, the film–fluid system is not expected to exhibit such uniformity. Duval et al.,[90] for a thermoresponsive thin film, and Yezek et al.,[60] on a previously studied system,[60,88] remove the assumption of a sharp interface between the charged film and the fluid, instead describing the interface with a continuous transition from a uniform charged region to the uncharged bulk fluid. Considering the latter, Yezek et al.[60] describe a previously studied system[87,88] with both the Ohshima and Kondo[53] uniform-charge model and a gradual decay model of the interface. There, measurements of streaming current disagree with the Ohshima theory in the low ionic strength region. The best theoretical fit to the data is obtained in regions of high ionic strength – it is in this limit of high ionic strength where the fluid penetration parameter, λ^*, is determined from a fit. The authors reason the inability of the model to match the experimental data over the entire range of ionic strength as an artifact of film rheology; the parameter fit for λ^* does not vary over the range of ionic strength, even as δ is dependent upon the ionic strength of solution.[60] Yezek et al. further analyzes the data using a continuous transition of charge/polymer volume fraction of the form:

$$\frac{\varphi^*(x)}{\varphi^{*\max}} = \frac{1}{2}\left(1 - \tanh\left(\frac{x-\delta}{\alpha}\right)\right) \qquad (55)$$

where $\varphi^{*\max}$ is the polymer volume fraction of the bulk gel (also the maximum value) and α is a length scale used to describe the diffuseness of the interface. For a sharp transition, $\alpha \to 0$. The fit of this parameter, α, for the streaming potential data shows a wide scatter over the range of solution concentrations and film densities tested. The parameter does, however, vary inversely with solution salt concentration, suggesting that the layer expands and contracts with changes in ionic strength. The Yezek et al.[60,88] studies suggests that $\alpha \to 0$ at high ionic strength. Thus, for variable property films, the high salt limit provides a subset of experimental space where thickness-independent parameters such as pH-dependent total film charge may be estimated. A drawback in their analysis, however, is the decoupled nature of α and λ^* in the fitted models. In their approach, Yezek et al.[60] assume a constant λ^* over the entire range of pH and ionic strength, while α is permitted to vary over the same range. Duval et al.[90] consider hydrodynamic screening with an uncharged temperature-sensitive hydrogel (poly(*N*-isopropylacrylamide)-*co*-*N*-(1-phenylethyl) acrylamide) grafted on a Teflon AF surface within an electrokinetic cell. They apply a theory developed in the same work[90] in which flow is permitted within the gel layer and fit streaming current data over a range of pH for films above and below a gel-swelling temperature threshold. Furthermore, the model permits a fixed potential or charge at the solid surface.

The Duval et al.[90] theory provides a good match to the observed streaming potential data, fitting only the parameters λ_o and α (taken $\to 0$) for the film over the entire range of pH. As the film is uncharged, there is no need to characterize charge density

or dissociation. The potential of the backing Teflon surface, however, was characterized separately, and used as a model input. When varying the ionic strength at fixed pH, Duval et al.[90] find agreement between the theory and experimental data (except for 15% deviation at low ionic strength), all while using the same value of hydrodynamic penetration within collapsed and expanded films over all values of ionic strength tested (from 0.01 to 10 mM KCl). This material was later studied with streaming current (and other techniques) by Cordeiro et al.,[91] although the focus there was the polymer film itself and not electrokinetic behavior.

Zimmermann et al.[92] executed electrokinetic investigations on poly(styrene)–poly(acrylic acid) (PS–PAA, charged) and poly-(styrene)–poly(ethylene oxide) (PS–PEO, uncharged) polymer brushes. Here, the authors measure streaming current, streaming potential, and conductivity of the films. Using literature values, the authors calculate the Donnan and surface potentials of the PS–PAA brush at full dissociation and report values of −186 and −161 [mV] (applying the Ohshima and Kondo theory[53]). The authors further implemented a standard Smoluchowski treatment to their streaming current data at high (i.e., fully dissociated) pH and find a value of $\zeta = -60$ [mV], highlighting the inability of the standard theory to capture the potential state of the film. Using the Bikerman surface conductivity formulation, they estimate a 7% contribution of the diffuse layer conductivity to the surface conductivity as a whole. For the uncharged PS–PEO diblock polymer brush, they find a negative surface potential, which they attribute to the polystyrene surface beneath the poly(ethylene oxide) brush layer. In examining this system, they measured the ζ-potential in the presence and absence of the graft poly(ethylene oxide) polymer brush and examined the results using the theory of Cohen Stuart et al.,[41,42] which assumes a transport-blocking polymer layer.

Understanding the full range of film properties involves deeper analysis than those presented so far – the state of a charged film depends on the pH and ionic strength of solution. In the prior analyses, rheological attributes of the film were assumed invariant upon changes in ionic strength, equivalent to changing the screening of charge within the film. Furthermore, no transition layer was assumed (i.e., $\alpha = 0$), although non-zero values of α are known to play an important role in measurable electrokinetic parameters.[58,59]

Toward resolving the interfacial structure, Zimmermann et al.[93] and Duval et al.[94,95] perform EK measurements on polymer films over a range of pH and ionic strength and relax the constraint of a sharp interface transition. Such an approach has been used previously to analyze human erythrocytes.[96] Zimmermann et al.[93] examine poly(N-isopropylacrylamid-co-carboxyacrylamid) films with streaming current/potential, conductivity, and ellipsometry measurements. Ellipsometry data was used to determine swelling as a function of pH for each value of salt concentration tested, and an analytical function was fit to these curves to develop an expression for film thickness. This function assumed the form:

$$\frac{\delta(\text{pH})}{\delta_o} = 1 + \frac{\delta_m - \delta_o}{2\delta_o}\left(1 - \tanh\left(\frac{\text{pH}_i^\delta - \text{pH}}{\Delta\text{pH}_i^\delta}\right)\right) \quad (56)$$

here, δ_m and δ_o represent film thickness at greatest and smallest extent, pH_i^δ is the pH at the inflection point of the δ–pH curve,

and ΔpH_i^δ is a characteristic width of the transition region at the inflection point. They further describe the diffuseness parameter of the interface (α) with a function having similar form and pH dependence:

$$\alpha = \frac{\alpha_m}{2}\left(1 - \tanh\left(\frac{\text{pH}_i^\alpha - \text{pH}}{\Delta\text{pH}_i^\alpha}\right)\right) \quad (57)$$

Thus, the model consists of six fit parameters: one parameter for the film charge density, one parameter for the hydrodynamic resistance of the film, one parameter for the dissociation constant of the charged groups in the film (pK_a), and three parameters to describe the diffuseness of the interface (α_m, pH_i^α, ΔpH_i^α). A fitting of ($\sim$13) pH points for each ionic strength is performed for streaming current coefficients ($\Delta I/\Delta p$) and surface conductivity data. The model fits obtained quantitatively match the relaxation behavior and magnitudes of the data. The authors show sensitivity of their result by displaying the best fit model along with variations in model parameters, which illustrates the necessity of the diffuse interface approach (i.e., non-zero α) to describe an interior extremum in the streaming current. Furthermore, the model recovered very nearly the maximum charge density within the film over three decades of ionic strength considered ($-\rho_f^{max}/F = 270$, 240, and 240 [mM] for 0.1, 1 and 10 mM of KCl). The approach does require different values of model parameters, however, for fits to streaming current and conductivity data. Values of the acid dissociation constant are higher by nearly one pH unit for conductivity versus streaming potential data. Also, the size of the relaxation in pH (ΔpH_α) varies as a function of ionic strength of the solution. In comparing model fits and parameter values between conductivity and streaming current data, Zimmermann et al.[93] remark on the measurement differences between the two techniques, specifically, that the pK_a value from streaming current measurements is consistently smaller than the same value inferred from conductivity measurements. In conductivity measurements, the technique is integrative across the entire film, whereas the streaming current measurement probes the film locally and is highly dependent upon the accessible surface layer of the film. This distance is characterized by the hydrodynamic penetration length of the fluid into the film. (The predicted penetration length is between about 1/80th and 1/200th of the measured film thickness.) Hence, the authors argue that the conductivity pK_a represents the bulk value across the entire film, while the streaming current value probes the pK_a of the surface layer. This argument is grounded in the analysis of Dukhin et al.[18] in which the electroosmotic component (dependent on film friction) is seen to be a small component of the conductivity in the film layer. They further claim that embedded acidic groups exhibit diminished dissociation owing to hydrophobicitiy of the film interior.

Duval et al.[94] extend the work by Zimmermann et al.[93] to examine covalently attached anionic poly(acrylic acid) (PAA) and cationic poly(ethylene imine) (PEI) films with similar techniques as before.[93] The authors successfully analyze the PAA and PEI films using the formalism developed previously – the PAA film shares many physical similarities to the previous system. The PEI film, however, possesses many differences that complicates the analysis. Ellipsometric swelling data is qualitatively different from the PAA film as a function of pH; the swelling data does not demonstrate a significant plateau at any extreme of pH.

Table 1 Collected electrokinetic characterization experiments with flows orthogonal, and parallel (*) to the surface normal of the diffuse interface. Here, materials with homogeneous microstructure on the scale of the electrostatic screening length are stressed; we do not include macro-porous membranes

Citation	Material type	Measurements performed[a]	Remarks
Afonso[97]*	Celgard N30F, Celgard NF-PES-10	SP	High flow rate imposed, ambiguous geometry; Smoluchowski-type ζ calculation
Ariza et al.[98]*	Commercial polysulfone membrane	C, SP	Smoluchowski type theory for measuring ζ, high surface conductivity
Fievet et al.[99]*	Sandwiched ceramic membranes	C, SP	Demonstrates importance of excess cell conductivity
Cohen Stuart et al.[42]	Poly(vinyl pyrrolidone) on glass	SP	Estimate hydrodynamic thickness of PVP film using a streaming potential measurement
Cordeiro et al.[91]	Poly(N-isopropylacrylamide-co-N-(1-phenylethyl) acrylamide)	AFM, CA, E, SC	Measure ζ; film exhibits temperature-dependent thickness; variable pH; films has no ionizable groups; attribute observed streaming current to adsorption of hydronium and hydroxide at underlying Teflon surface and subsequent screening of this charge by the polymer film
Duval et al.[90]	Poly(N-isopropylacrylamide)-co-N-(1-phenylethyl) acrylamide	SC	No charge units in hydrogel; show agreement with developed theory for rigid charged layer beneath the hydrogel and solution layers
Duval et al.[94]	Poly(ethylene imine), poly(acrylic acid)	C, E, SC	Extension of Zimmermann et al.[93] analysis. Poly(ethylene imine) film description is difficult due to swelling characteristics
Duval et al.[95]	Multilayer: poly(ethylene imine), poly(acrylic acid), bilayer lipid membrane	E, SC	Theory and experiments for non-homogeneous charge layer
Freudenberg et al.[89]	Cellulose film (native and crosslinked)	C, E, SC, SP	ϕ_D similar for crosslinked and uncrosslinked films, streaming current, swelling, and conductivity measurements differ
Voigt et al.[100]	Several polymers	SC, SP	Comparison of ζ from streaming current and streaming potential measurements
Yezek et al.[88]	Polyacrylamide gel	C, PT, SP	Measure ζ and ϕ_D as a function of ionic strength (NaCl), fluid convection within film neglected
Yezek et al.[60]	Polyacrylamide-co-sodium acrylate	C, SP	Implement non-uniform film charge model to describe experimental data
Yezek et al.[87]	Polyacrylamide-co-sodium acrylate	C	Extraction of conductance hindrance coefficient, implement of Dukhin, et al.[18,68] conductivity theory
Zimmermann et al.[92]	Poly(styrene)–poly(acrylic acid); poly(styrene)–poly(ethylene oxide)	C, SC, SP	Charged and uncharged diblock polymer brushes, estimate ϕ_D using charge dissociation model, ϕ_δ estimated with Ohshima theory, ζ based on Smoluchowski theory with Bikerman-type surface conductance
Zimmermann et al.[93]	Poly(N-isopropylacrylamid-co-carboxyacrylamid)	C, E, SC, SP	Apply diffuse interface model with transition layer, multi-parameter fit describes experimental data

[a] C – system/surface conductivity, CA – contact angle, E – ellipsometric film thickness, PT – potentiometric titration, SC – streaming current, SP – streaming potential.

Furthermore, the cationic polymer is polyprotic, with three pK_a values. The complication for the PEI film stems from ambiguity in describing the thickness of the diffuse interface and the rheological parameter for transport within the film, as the rheological parameter is typically estimated in a limit where the transition of the diffuse layer is minimal in size (or absent altogether). Returning to a point mentioned in Zimmermann et al.,[93] Duval et al.[94] attribute the difference in the conductance and streaming current fits of pK_a values for PEI and PAA films to changes in the chemical environment of the polymer by the plasma immobilization technique used to attach both polymers. The electrostatic model[93,94] of the interface uses a zero surface charge boundary condition at the solid surface.

We have discussed several experimental results that implemented (or developed) electrokinetic theories to extract physicochemical information on the state of the interface. The discussion is by no means exhaustive, serving mainly to illustrate applications of the theory developed in the previous sections, and regions of the experimental space where measurables of the theory diverge or are otherwise obscured by unknown system processes and parameters. The experiments discussed above, and several others which were not, are summarized in Table 1.

4 Discussion and conclusions

We have reviewed theoretical and experimental descriptions of electrokinetics at diffuse charged interfaces. Both theory and experiment reveal the importance of parameter space extrema in the description of these interfaces. In addition to an overview of theoretical and experimental studies, we considered EK coupling matrix formulations of diffuse fixed charge interfaces in specific limits of film thickness and potential.

Many considered theories and experiments rely upon simplifications in the governing physics; absent simplifications, full numerical solutions are often required. Simplifications follow when the Donnan potential $\phi_D^* \ll 1$, as the Poisson–Boltzmann equation can be linearized. Low Donnan potentials typically occur when the solution ionic strength is high. Other simplifications occur when the film is thick relative to the characteristic decay length of the electrical potential. Relative film thickness is influential for conductance calculations in the fixed charge layer, as curvature vanishes and the potential is assumed to be uniform in space. For films with electrical potential greater than the thermal voltage, or thickness not large relative to the Debye length, computational approaches must be implemented to analyze the system. Computational approaches are also necessary for systems with pH-dependent charge densities. These systems do simplify in limits of high and low dissociation, but the simplified expressions remain implicit in ϕ_D^*.

Future studies should account, in a more thorough way, for the influence of the electrokinetic boundary condition present at the plane of film attachment. The electrokinetic boundary value at a rigid surface is likely to be important, but is typically assumed to satisfy $\frac{d\phi}{dx}|_{wall} = 0$ (the exception is examined theoretically by Duval et al.[90]). In general, the ζ-potential of rigid materials responds in non-trivial ways to pH and ionic strength. Thus, the model-fitting method will fail unless the rigid material is well-characterized prior to experimentation with the soft interface (this amounts to the introduction of another free parameter for each combination of ionic strength and pH).

In a majority of the models presented, fluid properties within and outside the film are presumed identical – this assumption is called into question by the near constant potential within the thick film ($\delta^* \gg 1$), opportunity for large charge and ion concentration, and the effects of the polymer network itself. Furthermore, the thickness of the film suggests that, in contrast to a thin-EDL on a rigid surface, any inhomogeneity between charged and neutral regions can persist over a great extent (many times λ_d) magnifying the scope of inhomogeneous fluid property effects. Two cited exceptions to this simplification were the hindered mobilities of ionic species, and the dielectric constant of

the working fluid. Inhomogeneity in the dielectric constant has been considered in an *ad hoc* manner by some researchers,[48,49,54,55] with a range of dielectric constants selected to illustrate possible changes in system potential. These effects, the origin of which are discussed earlier, would be well treated by numerical methods owing to the complexity they introduce into the functional form of the governing equations.

Effects due to physical adsorption of electrolyte or other charge carriers (*e.g.*, hydronium, hydroxide) should also be considered in film layer charge models, especially for films with low dissociable charge densities. These and other field and concentration dependent properties introduce complications primarily through the functional form of the governing equation, and would be likely analyzed numerically. Further, the theories described often make use of a specific solution limit (high/low salt, high/low pH) to extract physical film parameters.[87,93,94] This approach is sufficient for cases in which film characteristics reach limiting values at experimental extremum; we communicated experimental evidence where this was not the case, however, and model values for the rheological behavior of the film could not be determined precisely.[94] There is area for improvement, then, in both theory and experiment for physical systems that do not as clearly exhibit constant or slowly varying properties in areas of high and low pH.

Acknowledgements

References

1 M. A. Swartz and M. E. Fleury, *Annu. Rev. Biomed. Eng.*, 2007, **9**, 229–256.
2 M. C. van Loosdrecht, J. Lyklema, W. Norde, G. Schraa and A. J. Zehnder, *Appl. Environ. Microbiol.*, 1987, **53**, 1898–1901.
3 H. H. Rijnaarts, W. Norde, E. J. Bouwer, J. Lyklema and A. J. Zehnder, *Colloids Surf., B*, 1995, **4**, 5–22.
4 A. T. Poortinga, R. Bos, W. Norde and H. J. Busscher, *Surf. Sci. Rep.*, 2002, **47**, 1–32.
5 F. Gaboriaud, M. L. Gee, R. Strugnell and J. F. L. Duval, *Langmuir*, 2004, **24**, 10988–10995.
6 D. Belder, H. Husmann and J. Warnke, *Electrophoresis*, 2001, **22**, 666–672.
7 D. Belder and M. Ludwig, *Electrophoresis*, 2003, **24**, 3595–3606.
8 G. Danger, M. Ramonda and H. Cottet, *Electrophoresis*, 2007, **28**, 925–931.
9 J. Israelachvili, *Intermolecular and Surface Forces*, Academic Press, 2nd edn, 1991.
10 W. B. Russel, D. A. Saville and W. R. Schowalter, *Colloidal Dispersions*, Cambridge University Press, 1st edn, 1989.
11 B. J. Kirby and E. F. Hasselbrink, *Electrophoresis*, 2004, **25**, 187–202.
12 B. J. Kirby and E. F. Hasselbrink, *Electrophoresis*, 2004, **25**, 203–213.
13 H.-J. Butt, B. Cappella and M. Kappl, *Surf. Sci. Rep.*, 2005, **59**, 1–152.
14 A. Pallandre, B. de Lambert, R. Attia, A. M. Jonas and J.-L. Viovy, *Electrophoresis*, 2006, **27**, 584–610.
15 M. Zembala, *Adv. Colloid Interface Sci.*, 2004, **112**, 59–92.
16 Z. Adamczyk, K. Sadlej, E. Wajnryb, M. Nattich, M. Ekiel-Jezewska and J. Blawzdziewicz, *Adv. Colloid Interface Sci.*, 2010, **153**, 1–29.
17 A. J. Bard and L. R. Faulkner, *Electrochemical Methods – Fundamentals and Applications*, Wiley, 2001.
18 S. S. Dukhin, R. Zimmermann and C. Werner, *J. Colloid Interface Sci.*, 2004, **274**, 309–318.

19 B. J. Kirby, *Micro- and Nanoscale Fluid Mechanics Transport in Microfluidic Devices*, Cambridge University Press, 2010.

20 R. J. Hunter, *Zeta Potential in Colloid Science: Principles and Applications*, Academic Press, 1981.

21 A. Delgado, F. Gonzlez-Caballero, R. Hunter, L. Koopal and J. Lyklema, *J. Colloid Interface Sci.*, 2007, **309**, 194–224.

22 C. Schwer and E. Kenndler, *Anal. Chem.*, 1991, **63**, 1801–1807.

23 W. Schutzner and E. Kenndler, *Anal. Chem.*, 1992, **64**, 1991–1995.

24 V. Tandon, S. K. Bhagvatula, W. C. Nelson and B. J. Kirby, *Electrophoresis*, 2008, **29**, 1092–1101.

25 V. Tandon, S. K. Bhagavatula and B. J. Kirby, *Electrophoresis*, 2009, **30**, 2656–2667.

26 P. J. Scales, F. Grieser, T. W. Healy, L. R. White and D. Y. C. Chan, *Langmuir*, 1992, **8**, 965–974.

27 C. Werner, H. Korber, R. Zimmermann, S. Dukhin and H.-J. Jacobasch, *J. Colloid Interface Sci.*, 1998, **208**, 329–346.

28 R. V. Wagenen and J. Andrade, *J. Colloid Interface Sci.*, 1980, **76**, 305–314.

29 J. T. G. Overbeek, *Colloid Science*, Elsevier, 1952, vol. 1.

30 J. T. Davies and E. K. Rideal, *Interfacial Phenomena*, Academic Press, 1963.

31 J. J. Bikerman, *Z. Phys. Chem., Abt. A*, 1933, **A163**, 378–394.

32 J. J. Bikerman, *Kolloid-Z.*, 1935, **72**, 100–108.

33 J. Lyklema, *Fundamentals of Interface and Colloid Science: Volume II Solid-Liquid Interfaces*, Elsevier, 1995.

34 J. Lyklema and M. Minor, *Colloids Surf., A*, 1998, **140**, 33–41.

35 H. P. Schwan and C. D. Ferris, *Rev. Sci. Instrum.*, 1968, **39**, 481–485.

36 R. J. Gross and J. F. Osterle, *J. Chem. Phys.*, 1968, **49**, 228–234.

37 T. Teorell, in *Transport Processes and Electrical Phenomena in Ionic Membranes*, ed. J. A. V. Butler and J. T. Randall, Pergamon Press, 1953, vol. 3, ch. 9, pp. 305–369.

38 H. Ohshima, *Adv. Colloid Interface Sci.*, 1995, **62**, 189–235.

39 J. F. L. Duval and H. Ohshima, *Langmuir*, 2006, **22**, 3533–3546.

40 J. Lyklema, *Fundamentals of Interface and Colloid Science: Soft Colloids*, Academic Press, 2005.

41 M. A. Cohen Stuart, F. H. W. H. Waajen and S. S. Dukhin, *Colloid Polym. Sci.*, 1984, **262**, 423–426.

42 M. Cohen Stuart and J. W. Mulder, *Colloids Surf.*, 1985, **15**, 49–55.

43 R. Zimmermann, S. Dukhin and C. Werner, *J. Phys. Chem. B*, 2001, **105**, 8544–8549.

44 J. K. Beattie, *Lab Chip*, 2006, **6**, 1409–1411.

45 E. Donath and V. Pastushenko, *Bioelectrochem. Bioenerg.*, 1979, **6**, 543–554.

46 E. Donath and V. Pastushenko, *Bioelectrochem. Bioenerg.*, 1980, **7**, 31–40.

47 P. C. Hiemenz, *Principles of Colloid and Surface Chemistry*, Marcel Dekker, 1977.

48 H. Ohshima and T. Kondo, *Biophys. Chem.*, 1990, **38**, 117–122.

49 H. Ohshima and S. Ohki, *Biophys. J.*, 1985, **47**, 673–678.

50 H. Ohshima and T. Kondo, *J. Colloid Interface Sci.*, 1988, **123**, 136–142.

51 R. W. Wunderlich, *J. Colloid Interface Sci.*, 1982, **88**, 385–397.

52 E. Donath and A. Voigt, *J. Colloid Interface Sci.*, 1986, **109**, 122–139.

53 H. Ohshima and T. Kondo, *J. Colloid Interface Sci.*, 1990, **135**, 443–448.

54 V. M. Starov and Y. E. Solomentsev, *J. Colloid Interface Sci.*, 1993, **158**, 159–165.

55 V. M. Starov and Y. E. Solomentsev, *J. Colloid Interface Sci.*, 1993, **158**, 166–170.

56 H. C. Brinkman, *Appl. Sci. Res.*, 1947, **A1**, 27–34.

57 H. Ohshima and T. Kondo, *J. Colloid Interface Sci.*, 1989, **130**, 281–282.

58 J. F. L. Duval and H. P. van Leeuwen, *Langmuir*, 2004, **20**, 10324–10336.

59 J. F. L. Duval, *Langmuir*, 2005, **21**, 3247–3258.

60 L. Yezek, J. Duval and H. van Leeuwen, *Langmuir*, 2005, **21**, 6220–6227.

61 P. Debye and A. M. Bueche, *J. Chem. Phys.*, 1948, **16**, 573–579.

62 A. E. Scheidegger, *The Physics of Flow through Porous Media*, University of Toronto Press, 1974.

63 J. Happel and H. Brenner, *Low Reynolds Number Hydrodynamics*, Kluwer, 1983.

64 S. S. Dukhin, R. Zimmermann, J. F. Duval and C. Werner, *J. Colloid Interface Sci.*, 2010, **350**, 1–4.

65 H. Ohshima and T. Kondo, *Colloid Polym. Sci.*, 1986, **264**, 1080–1084.

66 H. Ohshima and T. Kondo, *J. Colloid Interface Sci.*, 1987, **116**, 305–311.

67 L. Durlofsky and J. F. Brady, *Phys. Fluids*, 1987, **30**, 3329–3341.

68 S. S. Dukhin, R. Zimmermann and C. Werner, *J. Colloid Interface Sci.*, 2005, **286**, 761–773.

69 H. Ohshima, *Colloids Surf., A*, 1995, **103**, 249–255.

70 S. S. Dukhin, R. Zimmermann and C. Werner, *J. Colloid Interface Sci.*, 2008, **328**, 217–226.

71 P. H. Elworthy, A. T. Florence and A. Rahman, *J. Phys. Chem.*, 1972, **76**, 1763–1767.

72 H. C. Thomas and A. G. Langdon, *J. Phys. Chem.*, 1971, **75**, 1821–1826.

73 A. L. Iordanskii, A. L. Shterenzon, Y. V. Moiseev and G. E. Zaikov, *Russ. Chem. Rev.*, 1979, **48**, 781.

74 L. Masaro and X. Zhu, *Prog. Polym. Sci.*, 1999, **24**, 731–775.

75 T. Odijk, *Biophys. J.*, 2000, **79**, 2314–2321.

76 R. I. Cukier, *Macromolecules*, 1984, **17**, 252–255.

77 P. G. De Gennes, *Macromolecules*, 1976, **9**, 587–593.

78 F. Booth, *J. Chem. Phys.*, 1951, **19**, 391–394.

79 J. B. Hasted, *Aqueous Dielectrics*, Champan and Hall, 1973.

80 R. Paul and S. Paddison, *Solid State Ionics*, 2004, **168**, 245–248.

81 R. F. Probstein, *Physicochemical Hydrodynamics*, John Wiley, 2003.

82 G. Karimi and X. Li, *J. Power Sources*, 2005, **140**, 1–11.

83 G. Xie and T. Okada, *J. Electrochem. Soc.*, 1995, **142**, 3057–3062.

84 M. Elimelech, W. H. Chen and J. J. Waypa, *Desalination*, 1994, **95**, 269–286.

85 B. Teychene, P. Loulergue, C. Guigui and C. Cabassud, *J. Membr. Sci.*, 2011, **370**, 45–57.

86 T. Y. Chiu and A. E. James, *Colloids Surf., A*, 2007, **301**, 281–288.

87 L. Yezek, *Langmuir*, 2005, **21**, 10054–10060.

88 L. P. Yezek and H. P. van Leeuwen, *J. Colloid Interface Sci.*, 2004, **278**, 243–250.

89 U. Freudenberg, R. Zimmermann, K. Schmidt, S. H. Behrens and C. Werner, *J. Colloid Interface Sci.*, 2007, **309**, 360–365.

90 J. F. L. Duval, R. Zimmermann, A. L. Cordeiro, N. Rein and C. Werner, *Langmuir*, 2009, **25**, 10691–10703.

91 A. L. Cordeiro, R. Zimmermann, S. Gramm, M. Nitschke, A. Janke, N. Schafer, K. Grundke and C. Werner, *Soft Matter*, 2009, **5**, 1367–1377.

92 R. Zimmermann, W. Norde, M. A. Cohen Stuart and C. Werner, *Langmuir*, 2005, **21**, 5108–5114.

93 R. Zimmermann, D. Kuckling, M. Kaufmann, C. Werner and J. F. L. Duval, *Langmuir*, 2010, **26**, 18169–18181.

94 J. F. L. Duval, D. Kuttner, M. Nitschke, C. Werner and R. Zimmermann, *J. Colloid Interface Sci.*, 2011, **362**, 439–449.

95 J. F. L. Duval, D. Kuettner, C. Werner and R. Zimmermann, *Langmuir*, 2011, **27**, 10739–10752.

96 E. Donath, A. Budde, E. Knippel and H. Baumler, *Langmuir*, 1996, **12**, 4832–4839.

97 M. D. Afonso, *Desalination*, 2006, **191**, 262–272.

98 M. J. Ariza and J. Benavente, *J. Membr. Sci.*, 2001, **190**, 119–132.

99 P. Fievet, M. Sbai, A. Szymczyk and A. Vidonne, *J. Membr. Sci.*, 2003, **226**, 227–236.

100 A. Voigt, S. Wolf, S. Lauckner, G. Neumann, R. Becker and L. Richter, *Biomaterials*, 1983, **4**, 299–304.